Optical polarization modulation by competing atomic coherence effects in a degenerate four-level Yb atomic system

Sung Jong Park,[1,*] Chang Yong Park,[1] and Tai Hyun Yoon[2,†]
[1]*Korea Research Institute of Standards and Science, 1 Doryong, Yuseong, Daejeon 305-340, Korea*
[2]*Department of Physics, Korea University, Seoul 136-713, Korea*
(Received 1 February 2005; published 28 June 2005)

A scheme of optical polarization modulation of a linearly polarized infrared probe field is studied in a degenerate four-level Yb atomic system. We have observed an anomalous transmission spectra of two circular polarization components of the probe field exhibiting an enhanced two-photon absorption and a three-photon gain with comparable magnitude, leading to the lossless transmission and enhanced circular dichroism. We carried out a proof-of-principle experiment of fast optical polarization modulation in such a system by modulating the polarization state of the coupling field. The observed enhanced two-photon absorption and three-photon gain of the probe field are due to the result of competing atomic coherence effects.

DOI: 10.1103/PhysRevA.71.063819 PACS number(s): 42.50.Gy, 33.55.Ad, 42.50.Nn

Recently, there has been increasing interest in the study of nonlinear modification of the polarization state of light [1]. Especially, considerable attention has been given to Faraday rotation and nonlinear magneto-optical rotation (NMOR) in resonant atomic transitions [2,3]. While NMOR arises typically when light interacts with atoms in the presence of a magnetic field, laser-induced birefringence (LIB) resulting from atomic coherence has been observed without a magnetic field theoretically [4] and experimentally [5,6]. NMOR is also associated with quantum coherence effects—for example, coherent population trapping [7], electromagnetically induced transparency (EIT) [8], and electromagnetically induced absorption (EIA) [9].

Polarization rotation and coherent control in ladder-type three-level atomic systems have been demonstrated by use of pulsed lasers [3] and continuous-wave lasers [10]. In typical ladder systems [6,10], a probe field couples the ground state to the $m_J=\pm 1$ sublevels of the intermediate state and a driving field couples only the $m_J=+1$ (or $m_J=-1$) sublevel to the upper state. Thus, two circular polarization components (σ^+ and σ^- components) of the probe field experience different absorption and dispersion due to the difference of induced atomic coherence, leading to the recent observation of LIB in a wavelength-mismatched cascade system of inhomogeneously broadened Yb atoms [6]. Depending on the probe and coupling field intensities, the resultant absorption spectra for σ^+ and σ^- components may result not only in an EIT [11] but also in an EIA [6] spectrum. To achieve lossless transmission and large birefringence of the probe field, Wielandy and Gaeta used a detuned control field [10]. However, to facilitate lossless transmission and large circular dichroism of a resonant probe field, a net gain is required for one circularly polarized component, while the other component experiences enhanced absorption, as demonstrated in this study.

Here we investigate a scheme of optical polarization modulation in a medium composed of ${}^1S_0 \rightarrow {}^1P_1 \rightarrow {}^1S_0$ degenerate four-level Yb atoms exhibiting such an anomalous probe transmission. The level scheme in Fig. 1(a) is similar to the previously studied one in Refs. [4,6], but, distinctly, a strong probe field couples the intermediate state to the upper state in order to realize a large circular dichroism with lossless transmission. Once the coupling field is on, two circular polarization components of the strong probe field experience competing quantum coherence effects associated with two three-level subsystems, a ladder and a Λ-type subsystem, since they also act as the coupling fields for these systems. Consequently, fast modulation of the probe field polarization would be possible by modulating the polarization state of the coupling field relying on this competing quantum coherence effects. Unlike polarization rotation originating from the LIB, we observed large circular dichroism facilitated by enhanced absorption and three-photon gain for two orthogonal circular polarization components of the probe field. Numerical solutions of the density matrix equations at the steady state are analyzed to explain the observed atomic coherence effects.

In our experiment, shown schematically in Fig. 1(b), two external-cavity diode lasers are tuned to the $(6s^2)^1S_0 \rightarrow (6s6p)^1P_1$ transition at 399 nm (coupling field) and the

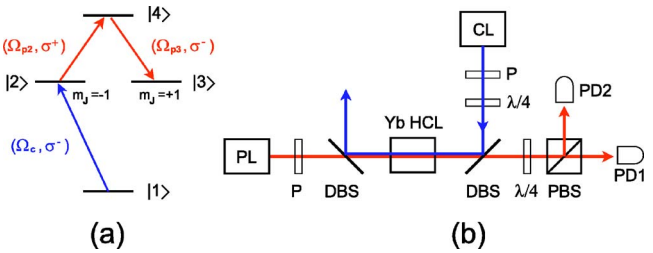

FIG. 1. (Color online) (a) Degenerate four-level system. $\Omega_{c(p2,p3)}$ and $\sigma^{+(-)}$ are Rabi frequencies and circular polarization states. Levels $|2\rangle$ and $|3\rangle$ are the Zeeman sublevels of the ${}^1P_1$ intermediate state with $m_J=-1$ and +1. (b) Schematic of the experimental setup. PL, probe laser; CL, coupling laser; P, polarizer; Yb HCL, Yb hollow cathode lamp; $\lambda/4$, quarter-wave plate; PBS, polarization beam splitter; PD, photo diode; DBS, dichroic beam splitter.

*Present address: National Measurement Institute, P.O. Box 264, Lindfield NSW 2070, Sydney, Australia.
†Electronic address: thyoon@korea.ac.kr

 ©2005 The American Physical Society

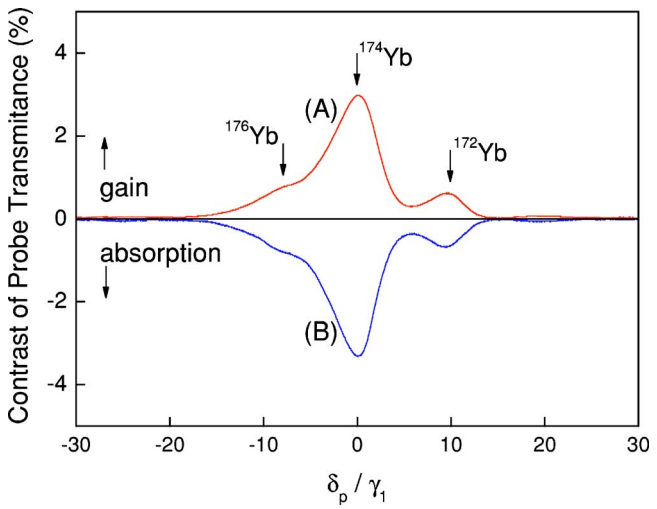

FIG. 2. (Color online) Measured contrast of probe transmission for $\sigma^-(A)$ and $\sigma^+(B)$ component versus δ_p/γ_1. The peaks correspond to three Yb isotopes are shown.

$(6s6p)^1P_1 \rightarrow (6s7s)^1S_0$ transition at 1077 nm (probe field). The probe laser is linearly polarized and the coupling laser is left-circularly polarized (σ^- polarization). Two Zeeman sublevels ($m_J = \pm 1$) in the intermediate $^1P_1$ state ($|2\rangle$ and $|3\rangle$) are coupled to the upper state ($|4\rangle$) by σ^+ and σ^- components of the probe field, and only the state $|2\rangle$ with $m_J = -1$ couples to the ground state $|1\rangle$ by the coupling laser. $\Omega_{i=c,p2,p3}$ are the Rabi frequencies. Levels $|2\rangle$ and $|3\rangle$ decay to the ground state $|1\rangle$ with the same rate $\gamma_1 = 2\pi \times 28$ MHz and level $|4\rangle$ decays to levels $|2\rangle$ and $|3\rangle$ with the same rate $\gamma_2 = 2\pi \times 3.5$ MHz. The coupling beam propagates along the opposite direction of the probe beam, and it is combined with and separated from the probe beam through a Yb hollow-cathode lamp by dichroic beam splitters. Individual laser intensities can be varied by separate half-wave plates and polarizers (not shown), and measured Rabi frequencies of each component of the probe and coupling field are $\sim 2\gamma_1$. To find the two-photon resonance condition, the coupling laser frequency is stabilized to the saturated absorption peak of the ^{174}Yb isotope [12] and the frequency of the probe laser is scanned across the upper transition such that two-photon resonance is reached. The probe transmission spectra corresponding to the two orthogonal polarization components are recorded and averaged simultaneously by a digital oscilloscope.

Figure 2 shows the measured contrasts of the transmission spectra of the two circular polarization components of the probe field as a function of δ_p/γ_1, where $\delta_p(\delta_c)$ is the probe (coupling) field detuning. Here, the contrast is defined such that the unity transmission corresponds to the detected probe power when the coupling laser is off. Three peaks associated with the three Yb isotopes are indicated by arrows. In Fig. 2, we can find two distinct features of the transmission spectra of the probe fields. First, the transmission curve (A) for σ^- component, which is resonant to the $|4\rangle - |3\rangle$ transition, exhibits gain spectrum, while the transmission curve (B) for σ^+ component, which is resonant to the $|4\rangle - |2\rangle$ transition, exhibits absorption spectrum. Second, the magnitudes of absorption and gain peaks are comparable so that the total field experiences a negligible absorption, demonstrating almost lossless transmission of the probe field at resonance. As much as 3.5% gain is measured for the σ^- component at 1077 nm in the presence of the coupling laser at 399 nm. We note that when the probe and coupling laser beams are copropagating, although the widths of the peaks are broadened significantly due to the Doppler effect so that the isotope spectrum merges into one peak, the gain at the line center is measured to be over 10%.

In Fig. 2, "0" in the abscissa corresponds to the two-photon transition frequency of the most abundant ^{174}Yb isotope with the velocity $v = 0$ along the propagation axis. The small peak at the right-hand (left-hand) side of the central peak is identified as the two-photon resonance signal associated with the ^{172}Yb(^{176}Yb) isotope. The frequency separation between different isotopes in Fig. 2 contains not only the isotope shift of the $(6s^2)^1S_0 \rightarrow (6s6p)^1P_1$ transition, but that of the $(6s6p)^1P_1 \rightarrow (6s6p)^1S_0$ transition which is not known. Thus, we calibrated the frequency unit in Fig. 2 by measuring the Doppler shift of the two-photon transition of ^{174}Yb by alternatively locking the frequency of the coupling laser from ^{174}Yb to ^{172}Yb single-photon transition and measuring the shifted two-photon resonance frequency of the ^{174}Yb isotope. Since the isotope shift of the ^{172}Yb at 399 nm is known—i.e., 534 MHz from ^{174}Yb [13]—the measured Doppler shift of the ^{174}Yb isotope at 1077 nm has the scaled value $k_2/k_1 \times 534$ MHz ~ 198 MHz $\sim 7\gamma_1$, where $k_1(k_2)$ is the wave vector of the coupling (probe) field. This shifted two-photon resonance condition is satisfied by the ^{174}Yb atoms with $v \sim 34$ m/s. In this way, the linewidth of the two-photon transition is measured to be about $4\gamma_1$.

The polarization state of the coupling field can be varied to any degree of polarization with a rotating polarizer and a quarter-wave plate, and can be modulated with high frequency with a ferroelectric liquid-crystal (FLC) polarization modulator (not shown in Fig. 1). To demonstrate the idea of polarization modulation, we carried out a proof-of-principle experiment; i.e., we changed abruptly the polarization state of the coupling field from the σ^- state to the σ^+ state. The change of polarization state of the coupling field resulted in the change of signs of the transmission spectra of curves A and B in Fig. 2 without altering the overall shape of the spectra. Furthermore, dynamical polarization modulation can easily be demonstrated by fast modulation of the polarization state of the coupling field with the FLC as explained. For instance, the demodulated detection of the modulated transmission signal of one circular polarization component by employing a lock-in amplifier allows us to directly measure the circular dichroism. We find that the measured spectrum of the circular dichroism shows the same spectrum as A in Fig. 2 without any distortion up to the tested modulation bandwidth of 10 kHz. We argue that the modulation bandwidth is, in principle, limited by the cycling time of the population in the closed four-level (diamond) system as in Fig. 1(a), where the life time of the spontaneous decay of 5.7 ns of the $(6s6p)^1P_1$ state limits the cycling time. Thus, in our degenerate four-level system, the polarization modulation bandwidth up to $\gamma_1/2\pi = 28$ MHz is envisaged. Such a fast modulation capacity of the atomic coherence would find in-

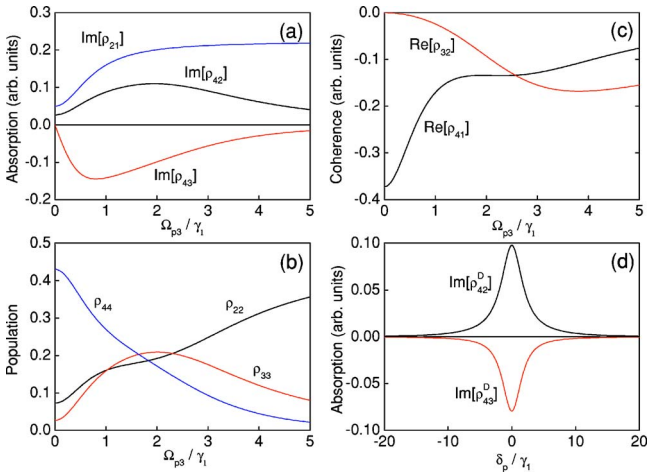

FIG. 3. (Color online) (a) Absorption $\mathrm{Im}[\rho_{21}]$, $\mathrm{Im}[\rho_{42}]$, and $\mathrm{Im}[\rho_{43}]$ versus Ω_{p3}/γ_1. (b) Population ρ_{44}, ρ_{22}, and ρ_{33} versus Ω_{p3}/γ_1. (c) Atomic coherence $\mathrm{Re}[\rho_{32}]$ and $\mathrm{Re}[\rho_{41}]$ versus Ω_{p3}/γ_1. (d) Doppler-averaged probe absorption $\mathrm{Im}[\rho_{42}^D]$ and $\mathrm{Im}[\rho_{43}^D]$ versus δ_p/γ_1. Parameters used are $\Omega_c=\Omega_{p2}=2\gamma_1$ for (a), (b), and (c) and $\Omega_c=\Omega_{p2}=\Omega_{p3}=2\gamma_1$ for (d), and $\delta_c=\delta_p=0$ for all graphs.

teresting applications—e.g., an all-optical switching and modulation [14].

Let us now discuss theoretically the atomic coherence effects in the degenerate four-level atomic system. The system that involves one degenerate transition is different from previously discussed four-level schemes [15], where the ground state is linked to a long-lived excited state by three-photon transitions. In our scheme, the final level $|3\rangle$ decays rapidly back to the ground state so that the interaction scheme is quite similar to the closed-loop configuration of a diamond geometry. Due to the relatively fast lifetime of the levels $|2\rangle$ and $|3\rangle$ with respect to the systems in Refs. [15,16], it is possible to increase the cycling time of the population in the diamond geometry, leading to the bandwidth enhancement of the polarization modulation. We now discuss the atomic coherence effects of our system based on the solutions of density matrix equations at steady state [6] to understand the quantum interference effects observed in our experiment.

If there is no probe field, of course, the intermediate sublevel $|2\rangle$ is populated by the coherent coupling field from the ground state $|1\rangle$. In the following, we consider resonant excitations only—i.e., $\delta_p=\delta_c=0$. With a nonzero Ω_{p2} and in the limit $\Omega_{p3}\rightarrow 0$, among the states $|1\rangle-|2\rangle-|4\rangle$ two-photon absorption occurs, causing population transfer from $|2\rangle$ to $|4\rangle$ without populating the intermediate state $|2\rangle$ [see Fig. 3(b) at $\Omega_{p3}\sim 0$]. In the strong probe field limit—i.e., $\Omega_{p2}\gg\Omega_c$—it is exactly corresponding to the conventional ladder-type EIT scheme, but here we consider the case where the coupling and probe fields are both strong—i.e., $\Omega_c\sim\Omega_{p2}\sim\gamma_1$ [6]. Moreover, when we apply the second probe field with Rabi frequency Ω_{p3}, there is increasing possibility to have a three-photon resonance from $|1\rangle$ to $|3\rangle$ that exhibits competing coherence effects. Actually, by analyzing the solutions of the density matrix equations, we find that the two-photon and three-photon resonances are, respectively, responsible for the observed enhanced absorption and gain of the probe fields in Fig. 2.

The gain-absorption coefficient for the probe field coupled to the transition $|2\rangle\rightarrow|4\rangle$ ($|3\rangle\rightarrow|4\rangle$) is proportional to $\mathrm{Im}[\rho_{42}]$ ($\mathrm{Im}[\rho_{43}]$), where $\mathrm{Im}[\rho_{ij}]$ ($\mathrm{Re}[\rho_{ij}]$) stands for the imaginary (real) part of the density matrix component ρ_{ij}. Figure 3(a) shows the absorption coefficients of the coupling and two components of the probe fields—i.e., $\mathrm{Im}[\rho_{21}]$, $\mathrm{Im}[\rho_{42}]$, and $\mathrm{Im}[\rho_{43}]$—as a function of Ω_{p3}/γ_1 with parameters $\Omega_c=\Omega_{p2}=2\gamma_1$. As Ω_{p3} becomes larger, the absorption of the probe field $\mathrm{Im}[\rho_{42}]$ increases at a similar rate as the coupling field absorption $\mathrm{Im}[\rho_{21}]$ for the range where $\Omega_{p3}\leqslant\Omega_{p2}$ and saturates at $\Omega_{p3}>\Omega_{p2}$, but never has a gain. This means that the second probe field enhances the two-photon absorption due to the quantum interference between the dressed states generated by the two strong probe fields and bare states $|2\rangle$, $|3\rangle$, and $|4\rangle$ [15]. Agarwal and Harshawardhan have shown that the two-photon absorption can be inhibited and enhanced using EIT in a four-level scheme [17] and this has been experimentally demonstrated by Gao *et al.* [18]. In their interaction schemes where the intermediate level is coupled to the two excited states, there exists a dressed state with two eigenstates; thus, the two transition pathways via two eigenstates could interfere. In our scheme, however, the enhanced two-photon absorption occurs due to the interferences among three different transition pathways via three eigenstates, making the interactions much more diverse. The important result of the dressed-state analysis in Ref. [15] is the prediction of the three-photon transition between levels $|1\rangle$ and $|3\rangle$. Therefore, we can conclusively say that the observed gain of the second probe field—i.e., $\mathrm{Im}[\rho_{43}]$ in Fig. 3(a)—originates from this three-photon process. The gain increases faster than the two-photon probe absorption $\mathrm{Im}[\rho_{42}]$ and reaches its maximum at $\Omega_{p3}\sim 0.8\gamma_1$.

Figure 3(b) shows the population distributions among the levels ρ_{44}, ρ_{22}, and ρ_{33} as a function of Ω_{p3}/γ_1 with the same parameters as in (a). Note that the gain at the second probe field occurs always with or without population inversion between levels $|4\rangle$ and $|3\rangle$ and we can see the maximum gain could be obtained at the population inversion condition—i.e., $\rho_{44}>\rho_{33}$ at $\Omega_{p3}\sim 0.8\gamma_1$. If we consider a Λ scheme composed of intermediate and upper states interacting with two probe fields, such a gain may be easily understood as a result of stimulated Raman transition. When the population distribution satisfies the condition $\rho_{22}\geqslant\rho_{44}$, called Raman inversion, the stimulated two-photon Raman process occurs following the $|2\rangle\rightarrow|4\rangle\rightarrow|3\rangle$ pathway. However, amplification of the probe field is revealed even under the condition $\rho_{22}\leqslant\rho_{44}$ for a certain parameter range where $\Omega_{p3}<1.8\gamma_1$. This indicates that a three-photon process dominates the observed gain in the second probe field over the two-photon Raman process.

For the resonant two-photon transitions, it is not difficult to show that the ladder-type two-photon coherence ρ_{41} and Λ-type two-photon coherence ρ_{32} are non zero and real. Thus, it is natural to expect some combined coherence effects from the two sub systems. One particular example of the combined coherence effect is the coexisting two-photon and three-photon resonances in the $|1\rangle$-$|3\rangle$ transition pathway, resulting in the enhanced absorption and gain of the probe field for $0<\Omega_{p3}<\Omega_c,\Omega_{p2}$. We depict the atomic co-

herence $\mathrm{Re}[\rho_{32}]$ and $\mathrm{Re}[\rho_{41}]$ as a function of Ω_{p3} in Fig. 3(c) to support such an argument. For instance, $\rho_{44} \gg \rho_{22}(\rho_{33})$ and $\mathrm{Re}[\rho_{41}]=-0.37(\mathrm{Re}[\rho_{32}]=0)$ at $\Omega_{p3}=0$—i.e., there exists a non zero two-photon coherence $\mathrm{Re}[\rho_{41}]$ due to the probe field, leading to the population inversion between levels $|4\rangle$ and $|2\rangle(|3\rangle)$. As Ω_{p3} increases, a Λ-type coherence starts to play an important role to create a three-photon transition from levels $|1\rangle$ to $|3\rangle$, leading to the population redistribution among three excited levels and the creation of novel coherence $\mathrm{Re}[\rho_{32}]$ between levels $|2\rangle$ and $|3\rangle$. The competition between the two atomic coherence effects develops with similar manner until $\Omega_{p3} \sim 2\gamma_1 = \Omega_c (= \Omega_{p1})$. In the intermediate parameter range where $\Omega_{p3} \sim 2\gamma_1$, however, the coherent interaction is fairly complicated since $\mathrm{Re}[\rho_{32}] \sim \mathrm{Re}[\rho_{41}]$ and no population inversion exists. It is interesting to note that for $\Omega_{p3} > 2.5\gamma_1$, $\rho_{22} > \rho_{33}$ and $-\mathrm{Re}[\rho_{32}] > -\mathrm{Re}[\rho_{41}]$, indicating the Λ-type coherence overwhelms the ladder-type coherence.

Finally, to confirm the experimental results, we illustrate the Doppler-averaged absorption spectra $\mathrm{Im}[\rho_{42}^{\mathrm{D}}]$ and $\mathrm{Im}[\rho_{43}^{\mathrm{D}}]$ in Fig. 3(d) as a function of δ_p/γ_1 at the parameters similar to the experimental conditions ($\Omega_c = \Omega_{p2} = \Omega_{p3} = 2\gamma_1$). As one can see, $\mathrm{Im}[\rho_{42}^{\mathrm{D}}]$ and $\mathrm{Im}[\rho_{43}^{\mathrm{D}}]$ exhibit enhanced absorption and gain spectra, supporting strongly the argument that the observed enhanced absorption and gain of the probe field is due to the result of competing coherence effects. As discussed above, the $|1\rangle \rightarrow |4\rangle$ two-photon transition gives rise to the enhanced absorption of the σ^+ component, while the $|1\rangle \rightarrow |3\rangle$ three-photon transition gives rises to the amplification of the σ^- component of the probe field. The calculated widths of the spectrum also agree with the experimentally observed narrow width of about $4\gamma_1$.

In summary, we introduced a scheme of optical polarization modulation of an infrared linearly polarized probe field in a degenerate four-level Yb atomic system. In our scheme, a lossless transmission of the infrared probe field is achieved, as the two circular polarization components experience enhanced absorption and gain with the comparable magnitude as a result of the competing coherence effects. In addition, the modulation bandwidth of the optical polarization is limited, in principle, by the recycling time of the population in a closed degenerate four-level system. The fast modulation capacity of the atomic coherence discussed in this paper would find interesting applications—e.g., an all-optical switching and modulation [14].

This research is supported by the Creative Research Initiatives Program of the Ministry of Science and Technology of Korea.

[1] D. Budker, W. Gawlik, D. F. Kimball, S. M. Rochester, V. V. Yashchuk, and A. Weis, Rev. Mod. Phys. **74**, 1153 (2002) and references therein; A. B. Matsko, I. Novikova, M. S. Zubairy, and G. R. Welch, Phys. Rev. A **67**, 043805 (2003).

[2] G. Labeyrie, C. Miniatura, and R. Kaiser, Phys. Rev. A **64**, 033402 (2001); D. Budker, D. F. Kimball, S. M. Rochester, and V. V. Yashchuk, Phys. Rev. Lett. **85**, 2088 (2000).

[3] P. F. Liao and G. C. Bjorklund, Phys. Rev. Lett. **36**, 584 (1976).

[4] A. K. Patnaik and G. S. Agarwal, Opt. Commun. **179**, 97 (2000); **199**, 127 (2001).

[5] F. S. Pavone, G. Bianchini, F. S. Cataliotti, T. W. Hänsch, and M. Inguscio, Opt. Lett. **22**, 736 (1997); H. S. Moon, D.-Y. Jeong, K.-H. Ko, and E. C. Jung, Opt. Commun. **228**, 133 (2003).

[6] T. H. Yoon, C. Y. Park, and S. J. Park, Phys. Rev. A **70**, 061803(R) (2004).

[7] M. O. Scully and M. S. Zubairy, *Quantum Optics* (Cambridge University Press, Cambridge, England, 1997).

[8] D. Budker, D. F. Kimball, S. M. Rochester, and V. V. Yashchuk, Phys. Rev. Lett. **83**, 1767 (1999); S. E. Harris, J. E. Field, and A. Imamoğlu, *ibid.* **64**, 1107 (1990).

[9] A. Lezama, S. Barreiro, and A. M. Akulshin, Phys. Rev. A **59**, 4732 (1999); F. Renzoni, S. Cartaleva, G. Alzetta, and E. Arimondo, *ibid.* **63**, 065401 (2001).

[10] S. Wielandy and A. L. Gaeta, Phys. Rev. Lett. **81**, 3359 (1998).

[11] K.-J. Boller, A. Imamoglu, and S. E. Harris, Phys. Rev. Lett. **66**, 2593 (1991).

[12] C. Y. Park and T. H. Yoon, Phys. Rev. A **68**, 055401 (2003).

[13] A. Banerjee, U. D. Rapol, D. Das, A. Krishna, and V. Natarajan, Europhys. Lett. **63**, 340 (2003).

[14] B. S. Ham, ETRI J. **23**, 106 (2001); B. S. Ham and P. R. Hemmer, Phys. Rev. B **68**, 073102 (2003).

[15] E. S. Fry, M. D. Lukin, T. Walther, and G. R. Welch, Opt. Commun. **179**, 499 (1999).

[16] T. Hong, C. Cramer, W. Nagourney, and E. N. Fortson, Phys. Rev. Lett. **94**, 050801 (2005).

[17] G. S. Agarwal and W. Harshawardhan, Phys. Rev. Lett. **77**, 1039 (1996).

[18] J.-Y. Gao, S.-H. Yang, D. Wang, X.-Z. Guo, K.-X. Chen, Y. Jiang, and B. Zhao, Phys. Rev. A **61**, 023401 (2000).